

SUPPORTING INFORMATION

Rb₂CdSi₄S₁₀: Novel [Si₄S₁₀] T2-Supertetrahedra-Contained Infrared Nonlinear Optical Material with Large Band Gap

Jiazheng Zhou[†], Zhongxu Fan[†], Kewang Zhang[†], Zhihua Yang, Shilie Pan* and Junjie Li*

Table of contents

1. Experimental procedures.....	3-5
2. Crystal data and structure refinements of $\text{Rb}_2\text{CdSi}_4\text{S}_{10}$	6
3. Atomic coordinates ($\times 10^4$), equivalent isotropic displacement parameters ($\text{\AA}^2 \times 10^3$) and BVS of $\text{Rb}_2\text{CdSi}_4\text{S}_{10}$	7
4. Selected bond lengths (\AA) and angles ($^\circ$) of $\text{Rb}_2\text{CdSi}_4\text{S}_{10}$	8-9
5. Anisotropic displacement parameters ($\text{\AA}^2 \times 10^3$) of $\text{Rb}_2\text{CdSi}_4\text{S}_{10}$	10
6. The typical PM chalcogenide IR NLO candidates with $E_g > 3.5$ eV.....	11
7. The HOMO-LUMO gap of the $[\text{M}(1)\text{S}_4]$ and $[\text{M}(2)_4\text{S}_{10}]$ ($\text{M}(1) = \text{Si, Ge, Sn, Ga}; \text{M}(2) = \text{Si, Ge, Ga}$) groups.....	12
8. The experimental and calculated XRD patterns of $\text{Rb}_2\text{CdSi}_4\text{S}_{10}$	13
9. The Raman spectrum of $\text{Rb}_2\text{CdSi}_4\text{S}_{10}$	14
10. The EDS spectrum, SEM image and mappings of $\text{Rb}_2\text{CdSi}_4\text{S}_{10}$	15
The RID measurements of $\text{Rb}_2\text{CdSi}_4\text{S}_{10}$	16
11. DSC curve of $\text{Rb}_2\text{CdSi}_4\text{S}_{10}$	17
12. PXRD patterns before and after heating at 800 °C of $\text{Rb}_2\text{CdSi}_4\text{S}_{10}$	18
13. Mulliken overlap population calculations of $\text{Rb}_2\text{CdSi}_4\text{S}_{10}$	19
14. References.....	20
15. Author contributions.....	20

Experimental Procedures

Reagents and Syntheses. All the raw reagents (RbCl, CdS, Si, S) with high purities ($\geq 99.99\%$) were commercially purchased by Aladdin Industrial Inc. and were stored in a dry Ar-filled glovebox with limited oxygen and moisture levels below 0.1 ppm. The $\text{Rb}_2\text{CdSi}_4\text{S}_{10}$ single crystal for structural determination was prepared by the flux method. The starting materials RbCl, CdS, Si and S were weighed and loaded into graphite crucibles with the ratio of 2 : 1 : 3 : 8. The silica tubes were sealed with methane-oxygen flame under a high vacuum of 10^{-3} Pa. After that, the sealed tubes were put into a computer-controlled furnaces and heating program setting to 600 °C in 20 h, kept at the temperature for 24 h, then the temperature was cooled to room temperature at a rate of 2.5 °C/h. Finally, the colorless single crystals for the title compound were harvested with a yield of about 90 %. The pure phases $\text{Rb}_2\text{CdSi}_4\text{S}_{10}$ powder samples were synthesized by solid-state reaction at 630 °C with stoichiometric ratio.

Single-Crystal X-ray Diffraction (XRD). High-quality transparent single crystals were selected under an optical microscope for collecting the X-ray diffraction data. A Bruker SMART APEX II CCD single crystal X-ray diffractometer using graphite-monochromatized molybdenum $\text{K}\alpha$ radiation ($\lambda = 0.71073 \text{ \AA}$) was performed to collect the crystal data at room temperature. After collection, the SADABS program was used to perform the multiscan-type absorption correction of the structure data. After that, the XPREP program in the SHELXTL program package was used to determine the space group, and the SHELXT and XL programs were applied to solve and refine the structure data by direct methods and full-matrix least-squares on F^2 . Finally, the PLATON program was used to check the possible missing symmetry elements, and no higher symmetry was found.^[1]

Energy-Dispersive X-ray Spectroscopy (EDS). The EDS spectrum and mapping of the title compound were characterized on a field emission scanning electron microscope (FE-SEM, JEOL JSM-7610F Plus, Japan) equipped with an energy-dispersive X-ray spectrometer (Oxford, X-Max 50), which was operated at 5 kV. The energy-disperse X-ray spectroscopy (EDS) analyses were carried out on a single crystal of $\text{Rb}_2\text{CdSi}_4\text{S}_{10}$. The EDS spectrum and mapping confirmed the existence of Rb, Cd, Si and S elements in the crystal with a quantified atomic ratio of 2.33 : 1 : 4.82 : 10, close to the stoichiometric ratio (2: 1: 4: 10)

Powder X-ray Diffraction (PXRD). To check the purity of pure phase powder samples, A Bruker D2 PHASER diffractometer with Cu $\text{K}\alpha$ radiation ($\lambda = 1.5418 \text{ \AA}$) was used to record the powder XRD pattern. The collected 2θ range was set to 10–70 ° with a scan rate of 0.02 °. The theoretical XRD pattern was calculated by Mercury software based on the CIF file of $\text{Rb}_2\text{CdSi}_4\text{S}_{10}$.

UV-Vis-NIR Diffuse Reflectance Spectroscopy and Infrared Spectroscopy. The optical diffuse-reflectance spectra of the title compounds were measured at room temperature using SolidSpec-3700DUV spectrophotometer in the wavelength range from 200 to 2600 nm. The collected data were converted to absorbance using the Kubelka-Munk function $F(R) = \alpha/S = (1 - R)^{2/2R}$ ($F(R)$: the ratio of absorption coefficient to scattering coefficient; α : absorption coefficient; R : reflectance; S : scattering coefficient) to figure out the band gap.^[2] The infrared spectroscopies for the polycrystalline $\text{Rb}_2\text{CdSi}_4\text{S}_{10}$, was measured by a Shimadzu IR Affinity-1 Fourier transform infrared spectrometer in the range of 2.5 – 25 μm , and KBr was used as a reference.^[3]

Raman Spectroscopy. $\text{Rb}_2\text{CdSi}_4\text{S}_{10}$ crystals were put on a transparent glass slide, and then a LABRAM HR Evolution spectrometer equipped with a CCD detector by a 532 nm radiation was applied to investigate the Raman spectrum in the 4000–100 cm^{-1} region. The strong absorption peaks around 369 cm^{-1} can be thought to be characteristic peaks of corner shared SiS_4 units. The three peaks at 155, 179 and 194 cm^{-1} should be related to the E, and T2 vibrational modes of the $[\text{SiS}_4]$ units, respectively. The peaks at 300 cm^{-1} and 605 cm^{-1} are attributed to the vibrations of $[\text{CdS}_4]$ units.^[4]

Thermal Analysis. Differential scanning calorimetry (DSC) was performed with a simultaneous NETZSCH STA 449C thermal analysis instrument. Approximately 15 mg of the polycrystalline powders were ground and then placed in a small silica tube that was subsequently sealed. The tube was heated from room temperature to 800 °C with a rate of 300 °C/h, and then cooled to room temperature with the heating/cooling rate both at 15 °C min^{-1} .

Refractive Index Difference (RID) Measurement. The RIDs of $\text{Rb}_2\text{CdSi}_4\text{S}_{10}$ were estimated by using the polarizing microscope equipped (ZEISS Axio Scope. 5 pol) with Berek compensator. Four small single crystals with different orientations were used for the characterization. The wavelength of the light source was 546 nm. The RID value is calculated by the following formula:

$$RID = \frac{\delta}{d} \quad (1)$$

where δ is the optical path difference, and d represents the thickness of the single crystal.

Second-Harmonic Generation (SHG) Measurement. The powder SHG measurement of $\text{Rb}_2\text{CdSi}_4\text{S}_{10}$ was characterized with the Kurtz–Perry method by a 2090 nm Q-switch laser. AgGaS_2 (AGS) was used as the reference. The title compound and AGS samples were ground and sieved into distinct particle size ranges (25–45, 45–63, 63–90, 90–125, 125–180, and 180–212 μm). The SHG signals were detected using a photomultiplier tube and recorded on an oscilloscope.^[5]

Laser-induced Damage Threshold (LIDT) Measurement. Micro-crystal samples of $\text{Rb}_2\text{CdSi}_4\text{S}_{10}$ with particle size range 25–45 μm were used to evaluate the LIDT under a pulsed YAG laser (1.06 μm , 5 ns, 10 Hz). AGS samples with similar size range were chosen as the reference. By adjusting the laser output energy, color change of the test samples were carefully observed by an optical microscope to determine the LIDT. The damaged energy E for AGS and $\text{Rb}_2\text{CdSi}_4\text{S}_{10}$ are 0.05 mj and 0.25 mj, respectively. The spot radius $r = 0.0225 \text{ cm}$, where r is the e^{-2} intensity radius. According to ISO 212541, the effective area of the Gaussian beam amounted to $A = \pi r^2/2 = 0.00024 \text{ cm}^2$.^[6] The LIDT of title compound was measured to be 208.3 MW/cm², which is 5 times than that of AGS

$$\frac{E}{\pi r^2 t}$$

(41.6 MW/cm²), from the formula: $LIDT = \frac{E}{\pi r^2 t}$, where E is the energy of a single pulse, r is the spot radius, and t is pulse width. Moreover, the static L (LIDT) behavior of title compound can also be estimated by comparing to the reference of AGS.^[7]

$$LIDT(\text{Rb}_2\text{CdSi}_4\text{S}_{10}) = LIDT(\text{AGS}) \times \frac{E(\text{Rb}_2\text{CdSi}_4\text{S}_{10})}{E(\text{AGS})} = LIDT(\text{AGS}) \times \frac{\frac{E(\text{Rb}_2\text{CdSi}_4\text{S}_{10})}{\pi r^2 t}}{\frac{E(\text{AGS})}{\pi r^2 t}} \cong 5 \times AGS \quad (2)$$

Theoretical Calculations. The band structure, total/partial density of states, and optical properties of $\text{Rb}_2\text{CdSi}_4\text{S}_{10}$ were calculated by using the plane-wave pseudopotential method implemented in the CASTEP based on the density functional theory (DFT) method. Perdew-Burke-Ernzerhof (PBE) exchange-correlation of Generalized Gradient Approximation (GGA) was applied in the calculation. The interactions between core and electron were described by the norm-conserving pseudopotential (NCP)^[8]. The Monkhorst-Pack schemes was set as $2 \times 4 \times 4$. The valence electrons were set as Rb 4p⁵ 5s¹, Cd 4p⁵, 4d¹⁰ 5s², Si 3s² 3p² and S3s² 3p⁴. Besides, The Heyd-Scuseria-Ernzerhof 06 (HSE06) hybrid functional was performed using the PWmat code, which runs on graphics processing unit processors (GPU). The pseudo-potential NCPP-SG15-PBE pseudo-potential and 50 Ryd plane wave cut-off energy was used in the calculation.

$$E_{XC}^{HSE} = \alpha E_X^{HF,SR}(\mu) + (1 - \alpha) E_X^{PBE,SR}(\mu) + E_X^{PBE,LR}(\mu) + E_C^{PBE} \quad (3)$$

(α : mixing parameter; μ : adjustable parameter controlling the short-range of the interaction; $E_X^{HF,SR}(\mu)$: short range Hartree-Fock exact exchange functional; $E_X^{PBE,SR}(\mu)$ and $E_X^{PBE,LR}(\mu)$: short and long range components of the PBE exchange functional; E_C^{PBE} : PBE correlation functional) In HSE06, the parameters are suggested as $\alpha = 0.25$.

The so-called length-gauge formalism originated by Aversa and Sipe was adopted to compute the SHG coefficients. The static SHG susceptibilities can be ascribed to virtual electron (VE) and virtual-hole (VH) processes. At a zero frequency, the formula of second-order NLO coefficients can be derived as:

$$\chi_{\alpha\beta\gamma}^{(2)} = \chi_{\alpha\beta\gamma}^{(2)}(VE) + \chi_{\alpha\beta\gamma}^{(2)}(VH) \quad (4)$$

$$\chi_{\alpha\beta\gamma}^{(2)}(VE) = \frac{e^3}{2\hbar m^3} \sum_{vv'c} \int \frac{d^3k}{4\pi^3} P(\alpha\beta\gamma) Im[P_{vv'}^\alpha P_{cv'}^\beta P_{cv}^\gamma] \left(\frac{1}{\omega_{cv}^3 \omega_{v'c}^2} + \frac{1}{\omega_{vc}^4 \omega_{cv'}^1} \right) \quad (5)$$

$$\chi_{\alpha\beta\gamma}^{(2)}(VH) = \frac{e^3}{2\hbar m^3} \sum_{vcc'} \int \frac{d^3k}{4\pi^3} P(\alpha\beta\gamma) Im[P_{cv'}^\alpha P_{cc'}^\beta P_{cv}^\gamma] \left(\frac{1}{\omega_{cv}^3 \omega_{vc}^2} + \frac{1}{\omega_{vc}^4 \omega_{cv'}^1} \right) \quad (6)$$

where, α , β and γ are the Cartesian components; v and v' are the denote valence bands; c and c' represent the denote conduction bands; $P(\alpha\beta\gamma)$ represents the denotes full permutation; $\hbar\omega_{ij}$ is the band energy difference; P_{ij} means the momentum matrix elements.^[9]

The electronic structure and optical properties of the $[M(1)S_4]$ and $[M(2)_4S_{10}]$ ($M(1) = Si, Ge, Sn, Ga; M(2) = Si, Ge, Ga$) groups were calculated by Gaussian 09 package under the condition of the B3LYP at LanL2DZ ([TMOF]).^[10] The atomic models were obtained from the known compounds.^[11] The result showed that, the HOMO-LUMO gap of aforementioned units is 5.326 eV for $[Si_4S_{10}]$, 4.48 eV for $[Ge_4S_{10}]$ and 5.57 eV for $[Ga_4S_{10}]$.

Table S1. Crystal data and structure refinements of $\text{Rb}_2\text{CdSi}_4\text{S}_{10}$.

Empirical formula	$\text{Rb}_2\text{CdSi}_4\text{S}_{10}$
Formula weight	716.30
Temperature (K)	303
Crystal system, space group	Orthorhombic, $Pna2_1$
Unit cell dimensions (Å)	$a = 18.6378(6)$ $b = 9.1309(3)$ $c = 10.6136(3)$
Volume (Å ³)	1806.22(10)
Z	4
Calculated density (Mg/m ³)	2.634
Completeness	99.2 %
Absorption coefficient (mm ⁻¹)	7.959
$F(000)$	1352
Goodness-of-fit on F^2	0.900
Final R indices ($F_o^2 > 2\sigma(F_o^2)$) ^a	$R_1 = 0.0265$, $wR_2 = 0.0564$
R indices (all data) ^a	$R_1 = 0.0331$, $wR_2 = 0.0638$
Absolute structure parameter	0.016(7)
Largest diff. peak and hole (e·Å ⁻³)	0.486 and -0.630
Flack parameter	0.016(7)

^a $R_1 = \sum ||F_o| - |F_c|| / \sum |F_o|$ and $wR_2 = [\sum w(F_o^2 - F_c^2)^2 / \sum wF_o^4]^{1/2}$ for $F_o^2 > 2\sigma(F_o^2)$

Table S2. Atomic coordinates ($\times 10^4$), equivalent isotropic displacement parameters ($\text{\AA}^2 \times 10^3$) and BVS of $\text{Rb}_2\text{CdSi}_4\text{S}_{10}$.

Atoms	x	y	z	U_{eq}	Wyckoff positions	BVS ^[a]
Rb(1)	8275(1)	-1454(1)	5009(1)	35(1)	4a	0.99
Rb(2)	4018(1)	1428(1)	7459(1)	42(1)	4a	0.86
Cd(1)	9140(1)	3378(1)	2553(1)	23(1)	4a	2.09
Si(1)	7662(1)	2698(2)	4712(2)	18(1)	4a	4.10
Si(2)	5968(1)	2683(2)	3451(2)	20(1)	4a	4.09
Si(3)	6192(1)	2117(2)	6591(2)	18(1)	4a	4.07
Si(4)	6499(1)	5517(2)	5343(2)	20(1)	4a	4.05
S(1)	5566(1)	1445(2)	5007(2)	23(1)	4a	2.03
S(2)	7603(1)	4996(2)	5015(2)	24(1)	4a	2.12
S(3)	8724(1)	2092(2)	4532(2)	22(1)	4a	2.02
S(4)	7061(1)	2051(2)	3097(2)	23(1)	4a	2.06
S(5)	5799(1)	1087(2)	8173(2)	23(1)	4a	1.98
S(6)	6077(1)	4414(2)	6957(2)	24(1)	4a	2.02
S(7)	6494(1)	7777(2)	5510(2)	24(1)	4a	1.97
S(8)	7305(1)	1561(2)	6372(2)	22(1)	4a	2.00
S(9)	5858(1)	4986(2)	3731(2)	26(1)	4a	2.03
S(10)	5426(1)	2103(2)	1838(2)	27(1)	4a	2.01
GII ^[b]						0.067

[a] The bond valence sum is calculated by bond-valence theory ($S_{ij} = \exp[(R_0 - R)/B]$, where R is an empirical constant, R_0 is the length of bond I (in angstroms), and $B= 0.37$).

[b] The global instability index (GII) calculated using

$$G = \sqrt{\frac{\sum_{i=1}^n (BVS - v_i)^2}{N}} \quad (7)$$

where N is the number of atoms in the formula unit. The GII is calculated as 0.067 which is lower than 0.2 indicating the rationality of the structure from this side.^[12]

Table S3. Selected bond lengths (Å) and angles (°) of Rb₂CdSi₄S₁₀.

Rb(1)-S(2)#6	3.4743(18)	S(3)#9-Rb(2)-S(1)	60.69(4)
Rb(1)-S(3)	3.383(2)	S(3)#9-Rb(2)-S(2)#9	54.86(4)
Rb(1)-S(4)#7	3.605(2)	S(3)#9-Rb(2)-S(4)#8	113.82(5)
Rb(1)-S(5)#2	3.437(2)	S(3)#9-Rb(2)-S(7)#10	136.22(5)
Rb(1)-S(6)#2	3.547(2)	S(3)#9-Rb(2)-S(8)#9	53.85(4)
Rb(1)-S(7)#6	3.434(2)	S(3)#9-Rb(2)-S(9)#10	89.51(5)
Rb(1)-S(8)	3.597(2)	S(3)#9-Rb(2)-S(10)#8	104.04(5)
Rb(1)-S(10)#7	3.372(2)	S(4)#8-Rb(2)-S(1)#8	54.16(4)
Rb(2)-S(1)	3.885(2)	S(4)#8-Rb(2)-S(1)	120.85(4)
Rb(2)-S(1)#8	3.846(2)	S(4)#8-Rb(2)-S(2)#9	59.17(4)
Rb(2)-S(2)#9	3.921(2)	S(4)#8-Rb(2)-S(8)#9	90.75(4)
Rb(2)-S(3)#9	3.432(2)	S(5)-Rb(2)-S(1)#8	65.57(4)
Rb(2)-S(4)#8	3.819(2)	S(5)-Rb(2)-S(1)	55.10(4)
Rb(2)-S(5)	3.420(2)	S(5)-Rb(2)-S(2)#9	140.30(5)
Rb(2)-S(7)#10	3.453(2)	S(5)-Rb(2)-S(3)#9	113.03(5)
Rb(2)-S(8)#9	3.860(2)	S(5)-Rb(2)-S(4)#8	113.34(5)
Rb(2)-S(9)#10	3.549(2)	S(5)-Rb(2)-S(7)#10	94.57(5)
Rb(2)-S(10)#8	3.450(2)	S(5)-Rb(2)-S(8)#9	155.88(5)
Cd(1)-S(3)	2.5279(19)	S(5)-Rb(2)-S(9)#10	86.36(5)
Cd(1)-S(5)#1	2.5621(19)	S(5)-Rb(2)-S(10)#8	70.46(5)
Cd(1)-S(7)#2	2.5297(19)	S(7)#10-Rb(2)-S(1)#8	62.60(4)
Cd(1)-S(10)#3	2.5511(19)	S(7)#10-Rb(2)-S(1)	146.35(5)
Si(1)-S(2)	2.125(3)	S(7)#10-Rb(2)-S(2)#9	120.28(5)
Si(1)-S(3)	2.065(3)	S(7)#10-Rb(2)-S(4)#8	82.14(5)
Si(1)-S(4)	2.132(3)	S(7)#10-Rb(2)-S(8)#9	87.23(5)
Si(1)-S(8)	2.151(3)	S(7)#10-Rb(2)-S(9)#10	57.81(5)
Si(2)-S(1)	2.137(3)	S(8)#9-Rb(2)-S(1)	114.33(5)
Si(2)-S(4)	2.150(3)	S(8)#9-Rb(2)-S(2)#9	53.38(4)
Si(2)-S(9)	2.134(3)	S(9)#10-Rb(2)-S(1)	101.70(4)
Si(2)-S(10)	2.057(3)	S(9)#10-Rb(2)-S(1)#8	110.40(5)
Si(3)-S(1)	2.136(3)	S(1)#8-Rb(2)-S(1)	108.90(2)
Si(3)-S(5)	2.059(3)	S(10)#8-Rb(2)-S(1)#8	55.72(4)
Si(3)-S(6)	2.144(3)	S(10)#8-Rb(2)-S(1)	69.67(4)
Si(3)-S(8)	2.148(3)	S(10)#8-Rb(2)-S(2)#9	76.45(4)
Si(4)-S(2)	2.140(3)	S(10)#8-Rb(2)-S(4)#8	54.20(4)
Si(4)-S(6)	2.137(3)	S(10)#8-Rb(2)-S(7)#10	117.32(5)
Si(4)-S(7)	2.071(3)	S(10)#8-Rb(2)-S(8)#9	129.49(5)
Si(4)-S(9)	2.143(3)	S(10)#8-Rb(2)-S(9)#10	156.24(5)
S(2)#6-Rb(1)-S(4)#7	65.33(5)	S(9)#10-Rb(2)-S(8)#9	74.26(4)
S(2)#6-Rb(1)-S(6)#2	109.46(5)	S(9)#10-Rb(2)-S(2)#9	126.96(5)
S(2)#6-Rb(1)-S(8)	122.15(5)	S(9)#10-Rb(2)-S(4)#8	137.23(5)
S(2)#6-Rb(1)-Si(2)#7	86.66(5)	S(3)-Cd(1)-S(5)#1	104.37(6)
S(3)-Rb(1)-S(2)#6	169.25(6)	S(3)-Cd(1)-S(7)#2	117.91(6)
S(3)-Rb(1)-S(4)#7	122.78(5)	S(3)-Cd(1)-S(10)#3	117.10(6)
S(3)-Rb(1)-S(5)#2	114.58(5)	S(7)#2-Cd(1)-S(5)#1	116.74(6)
S(3)-Rb(1)-S(6)#2	64.21(4)	S(7)#2-Cd(1)-S(10)#3	98.42(6)
S(3)-Rb(1)-S(7)#6	117.28(5)	S(10)#3-Cd(1)-S(5)#1	101.63(6)
S(3)-Rb(1)-S(8)	56.77(4)	S(2)-Si(1)-S(4)	111.62(11)

S(5)#2-Rb(1)-S(2)#6	64.70(5)	S(2)-Si(1)-S(8)	109.66(10)
S(5)#2-Rb(1)-S(4)#7	110.80(5)	S(3)-Si(1)-S(2)	109.16(11)
S(5)#2-Rb(1)-S(6)#2	57.14(4)	S(3)-Si(1)-S(4)	110.83(11)
S(5)#2-Rb(1)-S(8)	168.55(5)	S(3)-Si(1)-S(8)	104.08(10)
S(6)#2-Rb(1)-S(4)#7	166.90(5)	S(4)-Si(1)-S(8)	111.21(11)
S(6)#2-Rb(1)-S(8)	111.54(5)	S(1)-Si(2)-S(4)	108.96(11)
S(7)#6-Rb(1)-S(2)#6	57.37(4)	S(9)-Si(2)-S(1)	112.34(11)
S(7)#6-Rb(1)-S(4)#7	67.30(5)	S(9)-Si(2)-S(4)	112.33(11)
S(7)#6-Rb(1)-S(5)#2	116.07(5)	S(10)-Si(2)-S(1)	109.56(11)
S(7)#6-Rb(1)-S(6)#2	121.09(5)	S(10)-Si(2)-S(4)	104.52(11)
S(7)#6-Rb(1)-S(8)	66.96(4)	S(10)-Si(2)-S(9)	108.82(12)
S(8)-Rb(1)-S(4)#7	80.63(5)	S(1)-Si(3)-S(6)	111.69(11)
S(10)#7-Rb(1)-S(2)#6	83.88(5)	S(1)-Si(3)-S(8)	111.97(11)
S(10)#7-Rb(1)-S(3)	106.38(5)	S(5)-Si(3)-S(1)	108.44(11)
S(10)#7-Rb(1)-S(4)#7	56.86(4)	S(5)-Si(3)-S(6)	105.30(11)
S(10)#7-Rb(1)-S(5)#2	73.18(5)	S(5)-Si(3)-S(8)	108.85(11)
S(10)#7-Rb(1)-S(6)#2	111.61(5)	S(6)-Si(3)-S(8)	110.32(11)
S(10)#7-Rb(1)-S(7)#6	121.69(5)	S(2)-Si(4)-S(9)	110.85(11)
S(10)#7-Rb(1)-S(8)	115.37(5)	S(6)-Si(4)-S(2)	112.30(11)
S(1)-Rb(2)-S(2)#9	93.30(4)	S(6)-Si(4)-S(9)	109.17(11)
S(1)#8-Rb(2)-S(2)#9	112.00(4)	S(7)-Si(4)-S(2)	103.88(11)
S(1)#8-Rb(2)-S(8)#9	134.54(5)	S(7)-Si(4)-S(6)	113.53(11)
S(3)#9-Rb(2)-S(1)#8	159.58(5)	S(7)-Si(4)-S(9)	106.91(11)

Symmetry transformations used to generate equivalent atoms:

```
#1 -x+3/2,y+1/2,z-1/2; #2 -x+3/2,y-1/2,z-1/2; #3 x+1/2,-y+1/2,z; #4 x+1/2,-y-1/2,z;
#5 -x+1,-y,z-1/2; #6 x,y-1,z; #7 -x+3/2,y-1/2,z+1/2; #8 -x+1,-y,z+1/2; #9 x-1/2,-y+1/2,z;
#10 -x+1,-y+1,z+1/2; #11 x,y+1,z; #12 -x+3/2,y+1/2,z+1/2; #13 -x+1,-y+1,z-1/2;
```

Table S4. Anisotropic displacement parameters ($\text{\AA}^2 \times 10^3$) of $\text{Rb}_2\text{CdSi}_4\text{S}_{10}$.

Atoms	U^{11}	U^{22}	U^{33}	U^{23}	U^{13}	U^{12}
Rb(1)	39(1)	27(1)	39(1)	3(1)	6(1)	2(1)
Rb(2)	46(1)	41(1)	37(1)	0(1)	-2(1)	12(1)
Cd(1)	22(1)	23(1)	23(1)	0(1)	-1(1)	-1(1)
Si(1)	16(1)	18(1)	19(1)	-1(1)	0(1)	0(1)
Si(2)	17(1)	23(1)	19(1)	0(1)	-1(1)	-3(1)
Si(3)	18(1)	16(1)	20(1)	0(1)	2(1)	-2(1)
Si(4)	21(1)	16(1)	22(1)	-1(1)	2(1)	0(1)
S(1)	21(1)	24(1)	23(1)	0(1)	-1(1)	-4(1)
S(2)	21(1)	19(1)	33(1)	-3(1)	4(1)	-2(1)
S(3)	18(1)	25(1)	23(1)	3(1)	2(1)	1(1)
S(4)	18(1)	31(1)	22(1)	-6(1)	0(1)	0(1)
S(5)	27(1)	21(1)	20(1)	2(1)	4(1)	-2(1)
S(6)	34(1)	17(1)	21(1)	-3(1)	8(1)	1(1)
S(7)	31(1)	16(1)	26(1)	0(1)	8(1)	0(1)
S(8)	19(1)	22(1)	24(1)	3(1)	2(1)	1(1)
S(9)	30(1)	22(1)	27(1)	1(1)	-7(1)	0(1)
S(10)	21(1)	40(1)	20(1)	-2(1)	-3(1)	-7(1)

Table S5.The typical PM (experimentally verified) chalcogenide IR NLO candidates with $E_g > 3.5$ eV.

Compounds	SHG intensity (\times AGS)	Band gap	Ref.
LiGaGe ₂ S ₆	1.2	3.52	[13]
BaGa ₄ S ₇	1	3.54	[14]
LiInS ₂	0.6	3.59	[15]
[K ₃ Cl][Ga ₃ PS ₈]	1	3.6	[16]
BaB ₂ S ₄	0.7	3.61	[17]
Li ₂ Ga ₂ GeS ₆	1.2	3.65	[18]
[Rb ₃ Cl][Ga ₃ PS ₈]	1.1	3.65	[16]
Li ₂ BaGeS ₄	0.5	3.66	[19]
Na ₂ BaGeS ₄	0.3	3.7	[20]
Li ₂ SrGeS ₄	0.5	3.75	[21]
Li ₂ CdSiS ₄	1	3.76	[22]
Na ₂ SrGeS ₄	0.5	3.8	[21]
[K ₃ Br][Ga ₃ PS ₈]	1.2	3.85	[16]
[Ba ₄ Cl ₂][ZnGa ₄ S ₁₀]	1.1	3.85	[23]
SrNa ₂ SiS ₄	0.4	3.87	[24]
Li ₂ ZnSiS ₄	1.1	3.9	[25]
Na ₂ Ga ₂ SiS ₆	0.2	3.93	[26]
[KBa ₃ Cl ₂][Ga ₅ S ₁₀]	0.9	3.93	[27]
SrLi ₂ SiS ₄	0.4	3.94	[24]
BaAl ₄ S ₇	0.5	3.95	[28]
[RbBa ₃ C ₂][Ga ₅ S ₁₀]	0.93	3.95	[27]
[CsBa ₃ Cl ₂][Ga ₅ S ₁₀]	0.95	3.96	[27]
α -Li ₂ ZnGeS ₄	0.7	4.07	[29]
Li ₂ MgGe ₂ S ₇	0.6	4.12	[30]
LiGaS ₂	0.4	4.15	[31]
[Li ₂ Cs ₂ Cl][Ga ₃ S ₆]	0.7	4.18	[32]

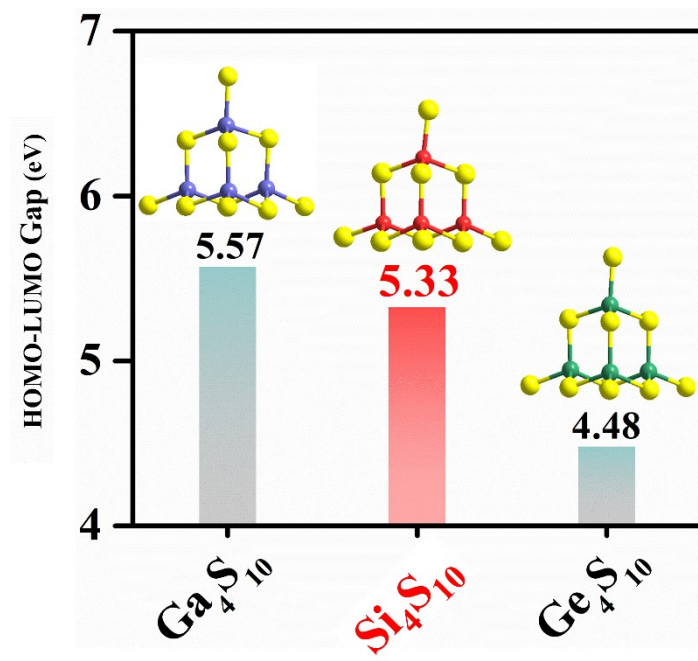


Figure S1. The HOMO-LUMO gap of the $[\text{M}(1)_4\text{S}_{10}]$ ($\text{M}(1) = \text{Ga}, \text{Si}, \text{Ge}$) groups.

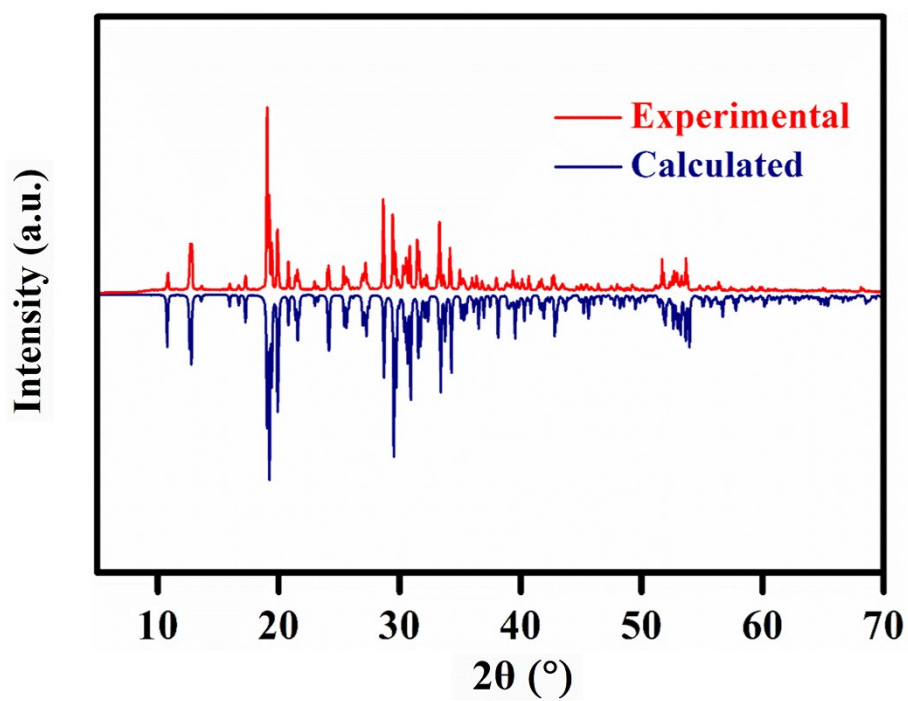


Figure S2. The experimental and calculated XRD patterns of $\text{Rb}_2\text{CdSi}_4\text{S}_{10}$.

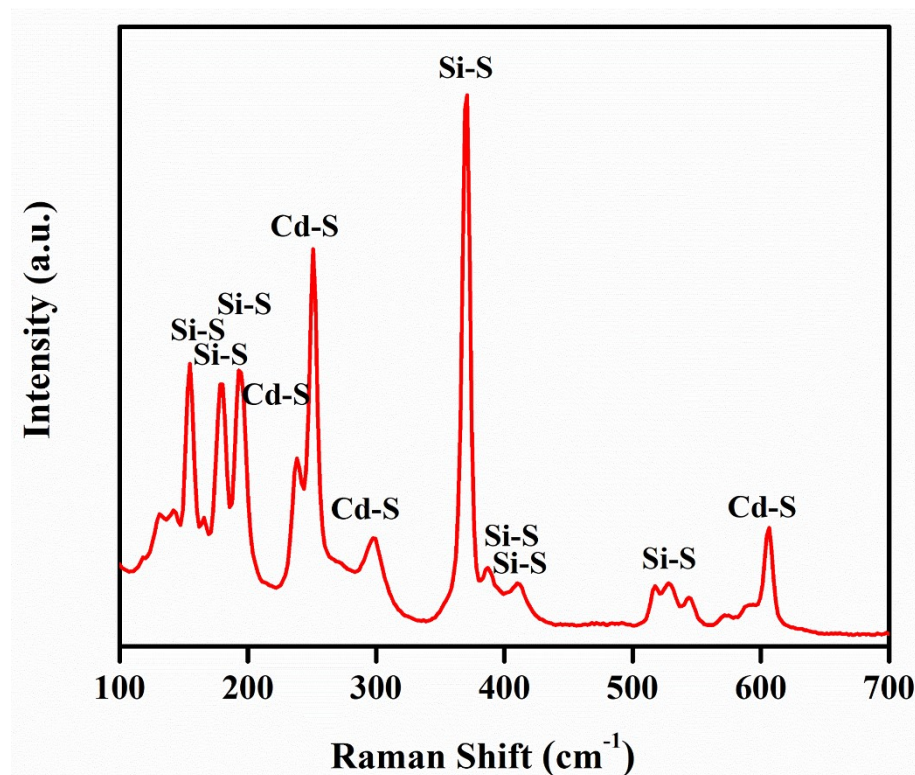


Figure S3. The Raman spectrum of $\text{Rb}_2\text{CdSi}_4\text{S}_{10}$.

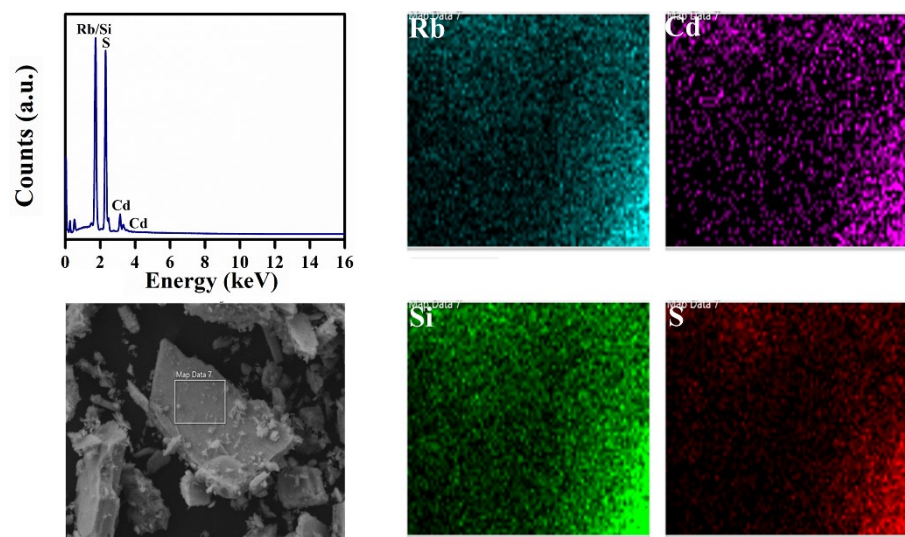


Figure S4. The EDS spectrum, SEM image and mappings of $\text{Rb}_2\text{CdSi}_4\text{S}_{10}$.

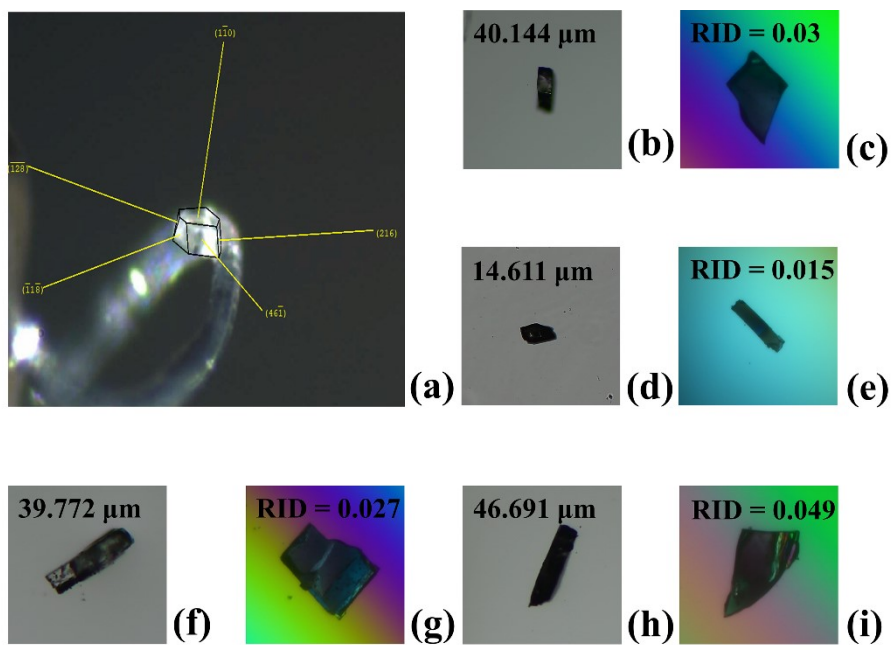


Figure S5. The RID measurements of $\text{Rb}_4\text{CdSi}_4\text{S}_{10}$. (a) The indices of crystallographic planes of crystal 1; (b, d, f, h) The thickness of the crystals 1-4 was measured using a microscope, which was 40.144, 14.611, 39.772 and 46.691 μm ; (c, e, g, i) The RID measurements on $\text{Rb}_4\text{CdSi}_4\text{S}_{10}$ crystals 1-4.

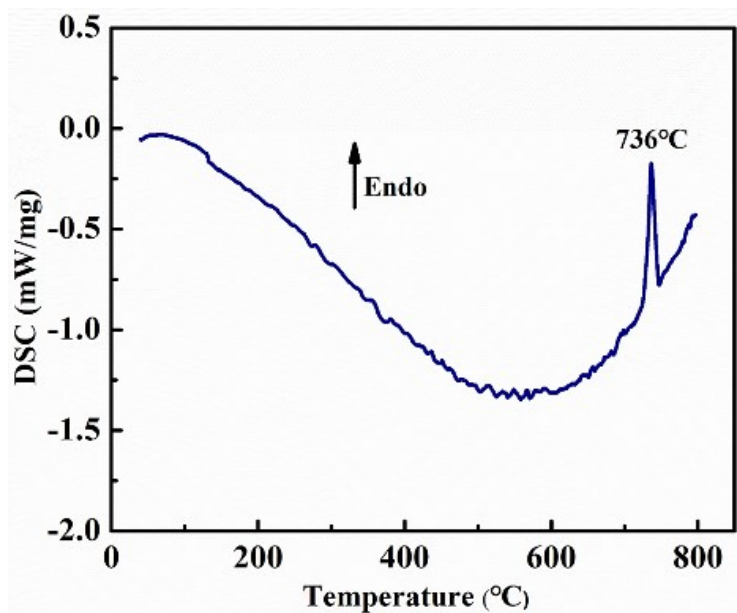


Figure S6. DSC curve of $\text{Rb}_2\text{CdSi}_4\text{S}_{10}$. The sharp endothermic peak at 736 °C on the heating curve can attribute to the decomposition of $\text{Rb}_2\text{CdSi}_4\text{S}_{10}$.

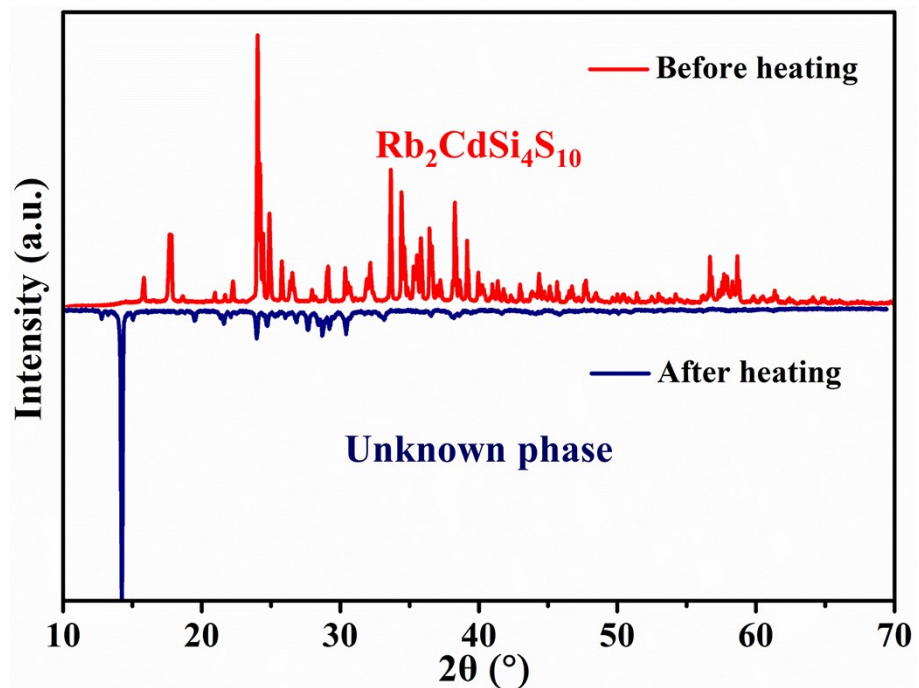


Figure S7. PXRD patterns before and after heating at 800 °C indicating the decomposition of $\text{Rb}_2\text{CdSi}_4\text{S}_{10}$ at high temperature. Based on the investigation in Inorganic Crystal Structure Database (ICSD - 4.7.0, the latest release of ICSD - 2021/10/25) and Jade 6, the main decomposed product could be a new phase.

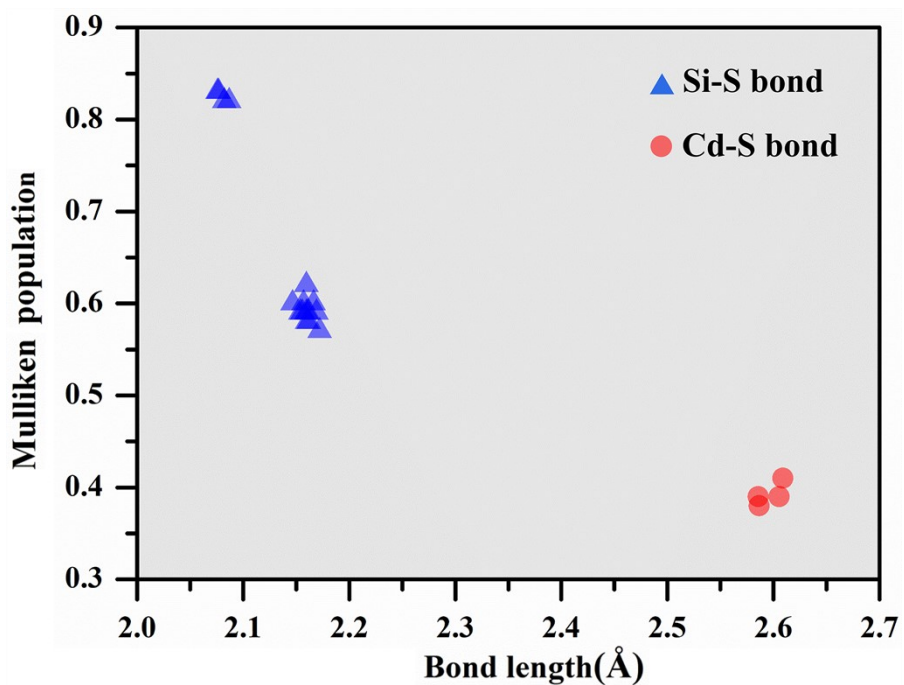


Figure S8. Mulliken population calculations of Rb₂CdSi₄S₁₀.

References

- [1] a) L. Haeming, G. M. Sheldrick, *Acta Crystallogr. Sect. A* **1999**, *55*, 206-206; b) G. M. Sheldrick, *Acta Crystallogr. Sect. A* **2008**, *64*, 112-122; c) A. L. Spek, *J. Appl. Crystallogr.* **2003**, *36*, 7-13.
- [2] G. Kortüm, Reflectance Spectroscopy, Springer, Berlin, **1969**.
- [3] Q. Q. Liu, X. Liu, L. M. Wu, L. Chen, *Angew. Chem. Int. Ed.* **2022**, *61*, e202205587.
- [4] a) R. Litran, R. Alcantara, E. Blanco, M. RamirezDelSolar, *J. Sol-Gel Sci. Technol.* **1997**, *8*, 275-283; b) G. D. Sun, G. H. Zhang, K. C. Chou, A. P. Dong, *Ind. Eng. Chem. Res.* **2017**, *56*, 12362-12368; c) L. J. Ma, M. C. Liu, D. W. Jing, L. J. Guo, *J. Mater. Chem. A* **2015**, *3*, 5701-5707; d) A. P. Litvinchuk, V. M. Dzhagan, V. O. Yukhymchuk, M. Y. Valakh, I. S. Babichuk, O. V. Parasyuk, L. V. Piskach, O. D. Gordan, D. R. T. Zahn, *Phys. Rev. B* **2014**, *90*; e) Y. Tokuda, T. Uchino, T. Yoko, *J. Non-Cryst. Solids* **2001**, *282*, 256-264; f) J. Liu, C. R. Wang, Q. Q. Xie, J. S. Cai, J. Zhang, *Nanoscale Res. Lett.* **2009**, *5*, 231-236; g) I. Hartenbach, I. Gerlach, T. Schleid, *Z. Anorg. Allg. Chem.* **2019**, *645*, 149-152.
- [5] S. K. Kurtz, T. T. Perry, *J. Appl. Phys.* **1968**, *39*, 3798-3813.
- [6] Y. Chu, P. Wang, H. Zeng, S. C. Cheng, X. Su, Z. H. Yang, J. J. Li, S. L. Pan, *Chem. Mater.* **2021**, *33*, 6514-6521.
- [7] a) X. Chen, Q. Jing, K. M. Ok, *Angew. Chem. Int. Ed.* **2020**, *59*, 20323-20327; b) J. H. Feng, C. L. Hu, B. X. Li, J. G. Mao, *Chem. Mater.* **2018**, *30*, 3901-3908.
- [8] a) J. P. Perdew, K. Burke, M. Ernzerhof, *Phys. Rev. Lett.* **1997**, *78*, 1396-1396; b) A. M. Rappe, K. M. Rabe, E. Kaxiras, J. D. Joannopoulos, *Phys. Rev. B* **1990**, *41*, 1227-1230; c) D. Vanderbilt, *Phys. Rev. B* **1990**, *41*, 7892-7895; d) J. Heyd, G. E. Scuseria, M. Ernzerhof, *J. Chem. Phys.* **2003**, *118*, 8207-8215; e) A. V. Krukau, O. A. Vydrov, A. F. Izmaylov, G. E. Scuseria, *J. Chem. Phys.* **2006**, 125.
- [9] C. Aversa, J. E. Sipe, *Phys. Rev. B* **1995**, *52*, 14636-14645.
- [10] M. J. Frisch, G. W. Trucks, H. B. Schlegel, G. E. Scuseria, M. A. Rob, J. R. Cheeseman, G. Scalmani, V. Barone, B. Mennucci, G. A. Petersson, H. Nakatsuji, M. Caricato, X. Li, H. P. Hratchian, A. F. Izmaylov, J. Bloino, G. Zheng, J. L. Sonnenberg, in *Gaussian 09, Rev. C.01*, Gaussian, Inc., Wallingford CT, **2010**.
- [11] a) J. Evers, P. Mayer, L. Möckl, G. Oehlinger, R. Köppe, H. Schnöckel, *Inorg. Chem.* **2015**, *54*, 1240-1253; b) A. Zeidler, J. W. E. Drewitt, P. S. Salmon, A. C. Barnes, W. A. Crichton, S. Klotz, H. E. Fischer, C. J. Benmore, S. Ramos, A. C. Hannon, *J. Phys.-Condens. Mat.* **2009**, *21*; c) Y. W. Guo, F. Liang, Z. Li, W. H. Xing, Z. S. Lin, J. Y. Yao, A. Mar, Y. C. Wu, *Inorg. Chem.* **2019**, *58*, 10390-10398; d) H. Lin, B. X. Li, H. Chen, P. F. Liu, L. M. Wu, X. T. Wu, Q. L. Zhu, *Inorg. Chem. Front.* **2018**, *5*, 1458-1462; e) M. Ribes, J. Olivier-Fourcade, E. Philippot, M. Maurin, *J. Mater. Chem.* **1973**, *8*, 195-205; f) G. Eulenberger, *Acta Crystallogr. Sect. B* **1976**, *32*, 3059-3063.
- [12] C. Preiser, J. Losel, I. D. Brown, M. Kunz, A. Skowron, *Acta Crystallogr. Sect. B* **1999**, *55*, 698-711.
- [13] D. Mei, S. Y. Zhang, F. Liang, S. G. Zhao, J. Q. Jiang, J. B. Zhong, Z. S. Lin, Y. D. Wu, *Inorg. Chem.* **2017**, *56*, 13267-13273.
- [14] X. S. Lin, G. Zhang, N. Ye, *Cryst. Growth Des.* **2009**, *9*, 1186-1189.
- [15] L. Isaenko, A. Yelisseyev, S. Lobanov, V. Petrov, F. Rotermund, J. J. Zondy, G. H. M. Knippels, *Mater. Sci. Semicond. Process.* **2001**, *4*, 665-668.
- [16] B. W. Liu, H. Y. Zeng, X. M. Jiang, G. E. Wang, S. F. Li, L. Xu, G. C. Guo, *Chem Sci* **2016**, *7*, 6273-6277.
- [17] H. Li, G. M. Li, K. Wu, B. B. Zhang, Z. H. Yang, S. L. Pan, *Chem. Mater.* **2018**, *30*, 7428-7432.
- [18] Y. Kim, I.-s. Seo, S. W. Martin, J. Baek, P. Shiv Halasyamani, N. Arumugam, H. Steinfink, *Chem. Mater.* **2008**, *20*, 6048-6052.
- [19] K. Wu, B. B. Zhang, Z. H. Yang, S. L. Pan, *J. Am. Chem. Soc.* **2017**, *139*, 14885-14888.
- [20] K. Wu, Z. H. Yang, S. L. Pan, *Angew. Chem. Int. Ed.* **2016**, *55*, 6713-6715.
- [21] K. Wu, Y. Chu, Z. H. Yang, S. L. Pan, *Chem. Sci.* **2019**, *10*, 3963-3968.
- [22] G. M. Li, Y. Chu, J. Li, Z. X. Zhou, *Dalton Trans.* **2020**, *49*, 1975-1980.
- [23] H. Chen, Y. Y. Li, B. X. Li, P. F. Liu, H. Lin, Q. L. Zhu, X. T. Wu, *Chem. Mater.* **2020**, *32*, 8012-8019.
- [24] Y. Yang, K. Wu, X. W. Wu, B. B. Zhang, L. H. Gao, *J. Mater. Chem. C* **2020**, *8*, 1762-1767.
- [25] G. M. Li, Y. Chu, Z. X. Zhou, *Chem. Mater.* **2018**, *30*, 602-606.
- [26] W. L. Xie, Y. H. Yun, L. H. Deng, G. M. Li, S. L. Pan, *Inorg. Chem.* **2022**, *61*, 7546-7552.
- [27] B. W. Liu, H. Y. Zeng, X. M. Jiang, G. C. Guo, *CCS Chem.* **2021**, *3*, 964-973.
- [28] D. J. Mei, J. Q. Jiang, F. Liang, S. Y. Zhang, Y. D. Wu, C. T. Sun, D. F. Xue, Z. S. Lin, *J. Mater. Chem. C* **2018**, *6*, 2684-2689.
- [29] J. H. Zhang, D. J. Clark, J. A. Brant, K. A. Rosmus, P. Grima, J. W. Lekse, J. I. Jang, J. A. Aitken, *Chem. Mater.* **2020**, *32*, 8947-8955.
- [30] A. Abudurusuli, J. B. Huang, P. Wang, Z. H. Yang, S. L. Pan, J. J. Li, *Angew. Chem. Int. Ed.* **2021**, *60*, 24131-24136.
- [31] V. V. Atuchin, L. I. Isaenko, V. G. Kesler, S. Lobanov, H. Huang, Z. S. Lin, *Solid State Commun.* **2009**, *149*, 572-575.
- [32] B. W. Liu, X. M. Jiang, B. X. Li, H. Y. Zeng, G. C. Guo, *Angew. Chem. Int. Ed.* **2019**, *59*, 4856-4859.

Author Contributions

Junjie Li and Shilie Pan designed and guided the experiment, and wrote the manuscript. Jiazheng Zhou and Zhongxu Fan synthesized the samples, characterized the properties, and wrote the manuscript. Kewang Zhang carried out the DFT calculations. Zhihua Yang discussed the results.